Electromagnetic time reversal focusing of near field waves in metamaterials

Matthew J. Chabalko and Alanson P. Sample[a)]
Disney Research Pittsburgh, 4720 Forbes Avenue, Lower Level, Suite 110, Pittsburgh, Pennsylvania 15213, USA

(Received 21 October 2016; accepted 13 December 2016; published online 27 December 2016)

Precise control of electromagnetic energy on a deeply subwavelength scale in the near field regime is a fundamentally challenging problem. In this letter we demonstrate the selective focusing of electromagnetic energy via the electromagnetic time reversal in the near field of a metamaterial. Our analysis begins with fundamental mathematics, and then is extended to the experimental realm where focusing in space and time of the magnetic fields in the near field of a 1-Dimensional metamaterial is shown. Under time reversal focusing, peak instantaneous fields at receiver locations are at minimum ~200% greater than other receivers. We then leverage the strong selective focusing capabilities of the system to show individual and selective powering of light emitting diodes connected to coil receivers placed in the near field of the metamaterial. Our results show the possibility of improving display technologies, near field imaging systems, increasing channel capacity of near field communication systems, and obtaining a greater control of energy delivery in wireless power transfer systems. *Published by AIP Publishing.*
[http://dx.doi.org/10.1063/1.4973210]

Manipulation of electromagnetic (EM) energy in the subwavelength regime is a topic of broad interest to physicists and engineers alike. In the far field regime, a technique used to focus energy (with resolution even below the classical diffraction limit) at a desired point in space and time is known as the electromagnetic time reversal (TR).[1] Electromagnetic time reversal (TR) refers to the invariance of Maxwell's Equations even when time, t, is replaced by its negative, $-t$, which still produces a consistent set of Maxwell's equations. As a result of reciprocity, the evolution of the fields between a source and receiver can be "rewound" in time by using the aforementioned "$-t$" substitution.[2] Thus, signals observed by a receiver or receiver array can be recorded, reversed in time, and then rebroadcast into the channel from which they came where they then retrace their steps back to the source and constructively interfere to focus in space and time.[3]

In general, the TR focusing effect is more pronounced when the channel response between source(s) and receiver(s) is [are] dispersive.[1,4,5] In this letter, we seek to demonstrate a selective focusing of the EM energy using electromagnetic time reversal in the near field only, and so we desire a near field medium with a dispersive frequency response. The work here contrasts with the previous work that has demonstrated near field to far field conversion of EM energy, with TR then used to reverse the process yielding focusing at the original near field source,[6–10] ultimately giving way to systems capable of highly localized focusing and far field super-resolution (i.e., resolution below that of the classical diffraction limit) imaging.[11–13] In pursuit of our goal here, however, we leverage the properties of near field metamaterials (NF-MM) that have been shown to support the Fabry Perot type resonances of magnetostatic near field volume and surface waves,[14–17] and even display the near field multipath effects,[18] all in a deeply subwavelength regime. In this way, near field metamaterials are uniquely suited for use as a dispersive medium for demonstrating the electromagnetic time reversal in the near field.

While the image formation and focusing of energy are possible with MMs via a near field lensing effect,[19,20] control of this behavior relies on fixed MM topologies and on optimization for a single frequency.[21] In this work, however, we selectively and dynamically control the spatial focus of EM energy on subwavelength scales within the near field of a MM operating in the 40–50 MHz range, with the MM supporting magnetostatic waves with typical wavelengths in the range of 3–25 cm, depending on the excitation frequency.

First, we lay a mathematical foundation for TR, followed by experimental results that corroborate the theory of near field time reversal. Lastly, the utility of this technique is illustrated by selectively addressing 1 of 8 receivers coupled to the MM, Fig. 1(a). In this experiment the receiver loads are blue LEDs that can be selectively turned on by using TR to focus energy at any desired LED's receiver. To add an intuitive and physical appreciation of the EM focusing we are pursuing, a qualitative plot (which is the result of an actual electromagnetic finite element based time reversal simulation) of the time reversal focused magnetic fields above a 1D NF-MM is shown in Fig. 1(b). The source is the *rightmost coil*, but by using TR, we have forced focusing to take place a little farther than half way down the slat (having arbitrarily chosen which coil to focus on), as indicated at the [passive] receiver location by the high density of flux lines as well as the high intensity of the magnetic field component directed normal to the slat (indicated by the dark blue coloring). This picture, showing the focusing of flux at an arbitrary location, is exactly what we achieve at any one of the 8 receiver locations used in this work by using the TR process.

The analysis we are about to undertake is in fact very general and applies to the near and far field TR systems

[a)]Electronic mail: alanson.sample@disneyresearch.com

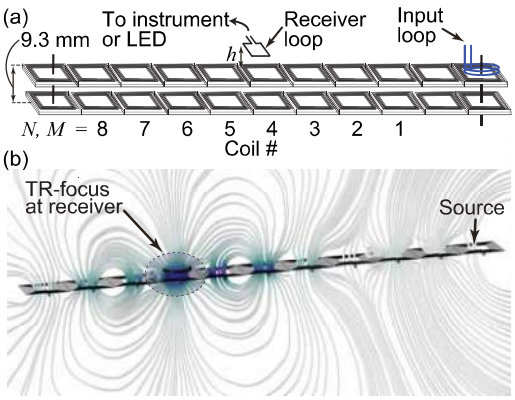

FIG. 1. (a) Setup of the MM system used in the TR experiments of this work. (b) Simulated (using commercial finite element software Comsol Multiphysics) TR focusing for a single slat of coils of (a). Streamlines are magnetic flux density and are colored proportional to the magnitude of the magnetic flux component directed normal to the coils (Blue, large; Gray, small). This is a temporal snapshot of the magnetic flux at the instant when TR focusing occurs after having rebroadcast the TR impulse response between source (rightmost coil on the slat) and receiver (black circle above slat).

broadcasting between one or more transmitters and one or more receivers. These transmitters and receivers could be antennas, coupled coils, etc. However, to aid in developing a less abstract description here, we will be specific in using the 1D NF-MM setup of this work to describe the time reversal process. The results are equally valid (although more complicated) for 2D and 3D metamaterials.

The MM channel is shown in Fig. 1(a), and consists of a series of 2.5 cm printed circuit board (PCB) coils, closely spaced in a line of 11 coils total to form a slat. Two slats are placed directly one on top of the other forming a bundle of 2. Finally, two of these bundles are spaced 9.3 mm apart to form the total 1D MM. The exact design of the 1D MM was not a focus of this work (i.e., we did not optimize or characterize it), except that its construction was guided by the need to form a subwavelength, and dispersive near field medium. A source coil was placed atop the far right end of the 1D MM to couple to into it, Fig. 1(a). A photograph of the physical setup is also shown in Fig. 2(a).

To be explicit about our apparatus and its operation in the near field, we here note that the center frequency of operation is 44.25 MHz, with a corresponding free space wavelength of 6.8 m. If we use a standard approximation to where the near field ends of $\lambda/(2\pi)$, where λ is the free space wavelength, then the near field extends no farther than about 1 m, and we expect a very weak coupling to receivers outside this region. To confirm this, we used a Vector Network Analyzer

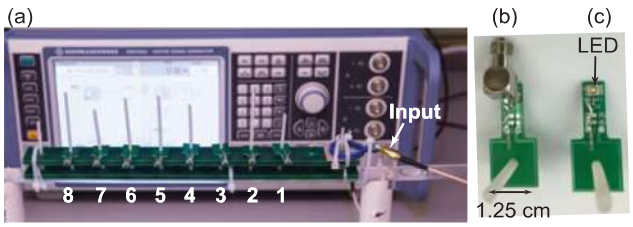

FIG. 2. (a) Photograph of the experimental apparatus of this work. (b) Close-up of the receiver loop used to collect the waveform data. (c) Same receiver as in (b) but with a blue LED attached as a load. The VSG is shown in the background of (a).

(VNA) to measure the transmission coefficient to a 7.6 cm diameter coil receiver located at 1 cm above the MM and 1 m above the MM. In the frequency band where the MM operates, we find $|S_{21}|$ is, at best, -7 dBm at 1 cm and, at best, -60 dBm at 1 m, thus the 5 orders of magnitude difference confirms that coupling to propagating waves from the device is negligible, and we have limited ourselves to the near field. Further, since the MM unit cells are composed of coil resonators, it is known that coupling to receivers drop off very quickly after the distance between the source and receiver is about 1 coil diameter.[22] Thus, for this work, we will be working very deep in the near field or within about 1 coil diameter (2.5 cm) of the MM, where the magnetic fields and coupling to receivers should be strongest.

Now, returning to establish the TR process used here, first consider the transmitter coil as it broadcasts a short pulse into the MM with N receiver locations above the MM, where, in this case, $N = 1, 2.8$. In the time domain, the short pulse, $p(t)$, is first applied to the blue input coil, and then the output at any one of the receivers is, mathematically, the convolution of the pulse with the channel impulse response between the source and that receiver, $h_N(t)$. Thus, in block diagram notation,

$$p(t) \rightarrow \boxed{h_N(t)} \rightarrow p(t) \otimes h_N(t), \tag{1}$$

where $\otimes$ is the convolution operator. After the impulse response is recorded at any one of the N receiver coil locations, this received signal is then reversed in time and rebroadcast through the channel. The response to the TR signal at some receiver coil, M (where N may or may not be equal to M), is then

$$\begin{aligned} a_N p(T-t) \otimes h_N(T-t) \rightarrow \boxed{h_M(t)} \rightarrow \\ [a_N p(T-t) \otimes h_N(T-t)] \otimes h_M(t), \end{aligned} \tag{2}$$

where T is a time delay to make the system causal, and a_N is a normalization constant which sets the time reversed signal's energy, and can be used to compensate for unrecoverable energy lost to heat (e.g., absorption by a conductor).

To be specific, the above two steps are implemented in this work by doing the following: First, a Gaussian pulse, $p(t)$, with full width half maximum (FWHM) bandwidth of 12.5 MHz, modulated at a carrier frequency of 44.25 MHz, and at a repetition rate of 3 μs is uploaded to the in-phase channel of a Vector Signal Generator (VSG). The signal is injected into the 1D MM via a source coil as shown in Fig. 1(a). Next, the In-phase and Quadrature channels (I and Q channels, respectively) of the pulse response at each of the 8 receiver locations in Fig. 1(a) is recorded using a single turn, 1.25 cm square, PCB pick-up coil [Fig. 2(b)], connected to a Vector Signal Analyzer (VSA). The recorded I and Q waveforms are then reversed in time, (the Q-channel's amplitude must also be flipped in sign to account for TR of the carrier), normalized, and then re-broadcast through the system via the same blue input coil. The I and Q pulse responses (original and time reversed) for two example coils (coil number $N = 2,7$) are shown in Fig. 3(a).

While the mathematical analysis in the time domain involves cumbersome convolution operators, the analysis

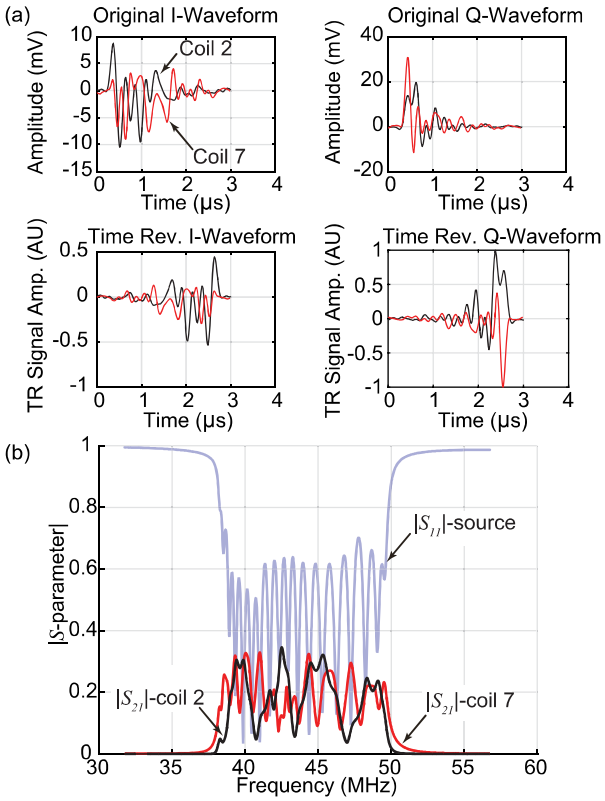

FIG. 3. (a) Example I and Q waveforms, along with the time reversed waveforms used in the experimental TR focusing system. (b) Measured *S*-parameter data showing the reflection coefficient, S_{11}, presented to the source as well as the transmission spectra, S_{21}, between the source and two receiver coils at positions 2 and 7 of Fig. 1(a).

becomes straightforward in the frequency domain where convolution is a simple multiplication. Thus, to gain an intuitive insight into the focusing effect of the TR process, we now recapitulate the analysis in the frequency domain, where the Fourier transform of the pulse, $P(\omega)$ (where ω is angular frequency) is first applied to the Nth channel with a frequency response $H_N(\omega)$, yielding

$$P(\omega) \rightarrow \boxed{H_N(\omega)} \rightarrow P(\omega)H_N(\omega). \tag{3}$$

In the frequency domain, TR is equivalent to phase conjugation;[23] thus, the time reversed signal is $a_N P^*(\omega)H_N^*(\omega)$, with * indicating the complex conjugate. After sending these frequency components back through the channel to be received at the Mth receiver, the final output, $V(\omega)$ is

$$\begin{aligned} &a_N P^*(\omega)H_N^*(\omega) \rightarrow \boxed{H_M(\omega)} \rightarrow \\ &\quad a_N P^*(\omega)H_N^*(\omega)H_M(\omega) = V(\omega). \end{aligned} \tag{4}$$

At the instant of focusing (which mathematically can be shown to be time $t=0$ in this analysis) the received signal's value [in this case voltage, $v(t)$] can be found using the inverse Fourier transform:

$$v(t=0) = \int_{-\infty}^{\infty} a_N P^*(\omega)H_N^*(\omega)H_M(\omega)\, d\omega. \tag{5}$$

Through Eq. (5), it can be seen that the key to focusing high or low energy (instantaneously) at any receiver M when sending the time reversed response of receiver N is to maximize the above integral for high energy and minimize it for low energy. This is essentially equivalent to maximizing or minimizing the cross-correlation between $H_N^*(\omega)$ and $H_M(\omega)$.

Optimally, for *completely* selective focusing energy at receiver N, two conditions need to be true: (1) when $N \neq M$, the channel responses of receiver N and M need to be orthogonal and thus Eq. (5) evaluates to 0 (i.e., their cross-correlation is zero), and (2) for $N=M$ the result should be non-zero (i.e., the channel autocorrelation is nonzero). In this way, energy is only focused at the Nth receiver (at the instant $t=0$) when transmitting the TR signal of that particular receiver.

Practically speaking, this optimal case cannot be exactly realized. Short of that, use of a dispersive medium (i.e., the NF-MM) can yield a system that has *relatively* orthogonal channels when $N \neq M$. Thus, a route becomes clear as to how energy can be maximized at receiver N when re-broadcasting its time reversed impulse response, while simultaneously assuring the energy received at the other M receivers is minimal. Lastly, we note that the above mathematics are only strictly true for the instant when focusing at the original ($N=M$) receiver takes place. At other instants in time, the received signal voltage at any coil may be higher or lower than those predicted by (5), but the net effect is that the more dissimilar the channel responses of coils N and M are, then the larger the ratio of the *peak* voltage of the desired receiver will be to the peak voltage observed at all other receivers, when looking over *all* time.

To again be explicit about the above using the physical system of this work, examples of the transmission coefficient, S_{21} between the source and receiver coils number 2 and 7 are shown in Fig. 3(b). Even without computation, the dissimilarity between the two spectra (i.e., their cross-correlation) is intuitively clear. Additionally, the dispersive nature of the MM used here is evident by noting the many modes present in the source's reflection coefficient spectrum, S_{11}. When designing the blue input coil, we adjusted the number of turns and its height above the MM such that S_{11} was as close to 0 as possible for as many of the modes seen as possible [see Fig. 3(b)]. By minimizing reflections across frequency, we are assured that as much power as possible is actually delivered to the MM in as many modes as possible, which can then participate in the TR focusing effect.

Quantitatively, we measured the transmission spectrum at all 8 receiver coil locations in Fig. 1(a) and then computed the integral in Eq. (5) for $N,M=1.8$. The results are represented in the matrix of Fig. 4(d), where the values have been normalized to the maximum value of the resulting 8×8 matrix. Along the diagonal, where $N=M$, the values are high, signifying a strong autocorrelation. On the other hand, the off-diagonal values are only small fractions of the diagonal values, signifying weaker cross-correlation. Taken together, the results of Fig. 4(d) all signify a highly dispersive NF system, suitable for exploiting TR to attain focusing in the near field. Below, we continue with a description of the experimental TR results.

After the time reversed channel pulse response from any coil N is sent back through the channel from the source coil,

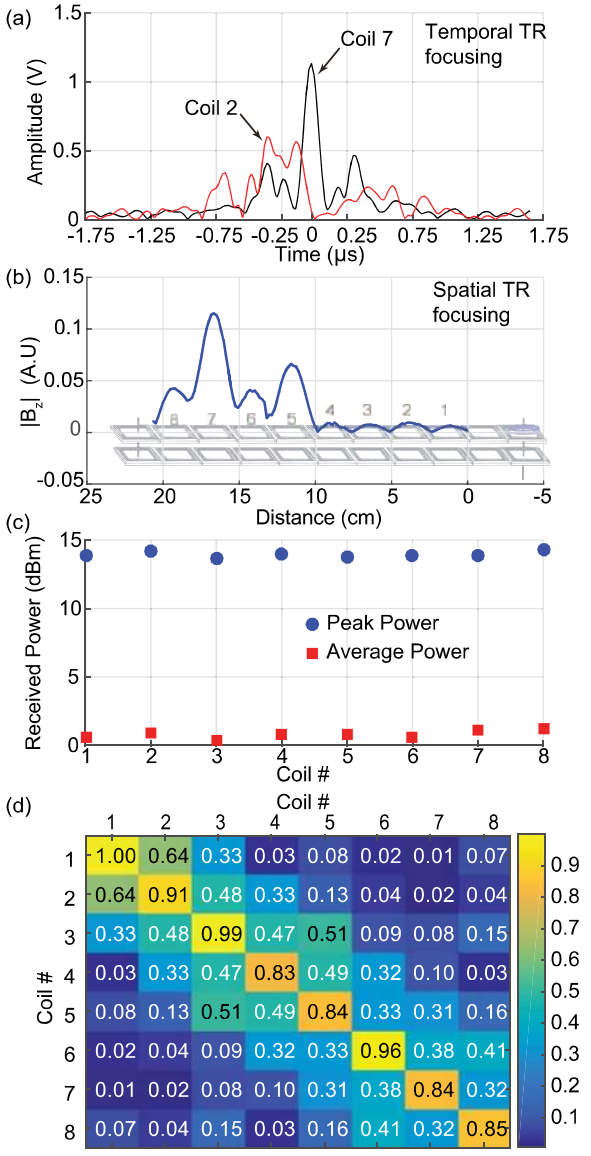

FIG. 4. (a) Example of temporal TR focusing when sending the TR waveform of coil number 7 back through the system. (b) Example of the spatial TR focusing: coil 7's TR waveform is broadcast from the receiver and a 3 mm diameter coil is scanned 7 mm above the MM surface. The flux at the instant of TR focusing is plotted as a function of position. (c) Peak and average power levels obtained by setting the individual heights of the 8 PCB receivers above the MM so that they have approximately the same values when their own TR signal is emitted from the source coil. (d) Matrix of values found by computing the integral in Eq. (5) after measuring the channel frequency response between the source and 8 receivers in Fig. 1(a).

TR focusing takes place at the same receiver coil, N. For the other M coils there is no focusing effect and the peak signal level is diminished compared to coil N. An example of this is shown in Fig. 4(a), where the received signal at coils 2 and 7 are plotted for the case when the time reversed signal of coil $N=7$ is sent back through the system. Here, strong temporal focusing at coil number 7 is evident. The *peak* voltage is almost twice that of coil number 2 (or almost 6 dB more power). At the instant of focusing ($t=0$), the ratio of received voltages is much larger.

Figure 4(b) goes further to illustrate the spatial TR focusing at the instant in time that the fields focus at coil number 7. To obtain this plot, once again coil number 7's time reversed impulse response is re-broadcast through the MM and then the flux density above the MM (7 mm above its surface) is recorded using a small sensing coil. This plot clearly indicates a peak magnetic flux density at the coil number 7's location when TR focusing occurs. This plot is essentially a 1-Dimensional magnitude slice of the scenario depicted in Fig. 1(b).

After all 8 channel responses were recorded, the VSG was programmed to output the same amount of power when re-broadcasting any of the TR impulse responses. As a normalization step, all 8 receivers had their height above the MM adjusted so that they each absorbed the same amount of power when their TR signal was sent; this is the separation h, of Fig. 1(a) between the MM coil and the square receiver loops. The result is plotted in Fig. 4(c). Adjusting the height between the output loops and the MM coils effectively increases (closer) or decreases (farther) the coupling between receiver and MM and hence the received signal strength. Thus, this amounts to regulating the total energy absorbed by the load when $N=M$ (i.e., autocorrelation energy), and is a way to make all 8 loads absorb the same energy when their TR signal is sent. This is a necessary step since NF-MM waves suffer attenuation as they propagate, so receivers that are laterally farther away from the source are disadvantaged in how much energy they receive, compared to receivers that are (laterally) closer to the source coil. For this initial study, we did not focus on what an optimal coupling from receiver to MM might be, but rather we were just seeking to ensure that all receivers got the same amount of power when their TR signal was sent, and adjusted the coupling experimentally to achieve this result, Fig. 4(c). In all experiments up to this point, the load was the 50 Ω port of the VSA. In a final experiment describe below, the load was changed to be a blue LED with measured "on" impedance of less than 10 Ω and a nearly 0 reactive impedance in the frequency band of operation. It is also worth mentioning that, under the condition that there is no load, the energy of the injected signal is dissipated by the metamaterial itself (specifically in the ohmic losses of the unit cell's copper coils). As mentioned earlier, energy loss to radiative modes is negligible as we are in a strongly near field regime.

To demonstrate the remarkably strong selective TR focusing ability of the simple MM used here, we placed the PCB receiver loops at the 8 locations of Fig. 1(a), but now connected to LED loads. The PCB loops were mounted on the threaded rods so that their height, h, above the MM could be adjusted. The heights were adjusted to be approximately the same as when the data of Fig. 4(c) was recorded, so they would receive approximately the same power when their TR signal was sent. Some fine tuning of their heights was necessary, but the result was that we were able to selectively turn on the LEDs with approximately the same brightness simply by sending the TR signal of whichever one was desired. The other LEDs did not visibly turn on except the one whose TR signal was broadcast. The selective turn-on and subsequent powering of a given LED is owed to the fact that the TR focusing in time pushes the selected LED above its turn-on threshold voltage for a brief period of time and so it emits light. Since we are replaying the TR signal of the desired receiver continuously (i.e., we replay the TR signal at a

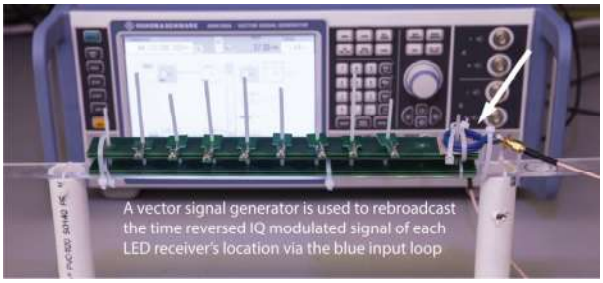

FIG. 5. This is a still image of the supporting online video that shows the selective powering of LEDs using TR focusing. Each LED is turned on by continuously sending the TR channel response of the desired LED. This signal is sent at a repetition rate of 3 μs and since the TR focused waveform pushes only the selected LED above its turn-on threshold voltage, only that LED appears to be on. The LED is turning on and off very fast due to the 3 μs repetition rate of the TR waveform, but to the human eye, it appears to be on continuously. (Multimedia view) [URL: http://dx.doi.org/10.1063/1.4973210.1]

repetition rate of 3 μs), the chosen LED appears to be on continuously to the human eye, even though it is actually flickering on and off at around 0.33×10^6/s. The other diodes do not turn on since they are, at all times, below the threshold unless their own time reversed channel response is sent. This is in accordance with Fig. 4(a) where, as an example, the focusing occurred at coil 7, but coil 2's peak voltage was, at its best, half that of the selected coil 7. A photo of the experimental LED setup, and a supplementary video illustrating the selective turn-on of each of the 8 LEDs, can be found linked from Fig. 5 (Multimedia view).

In this letter, we have demonstrated the electromagnetic time reversal in the near field to near field regime and demonstrated a strong focusing of the magnetic field above the surface of a metamaterial. Our results here have several implications for practical systems. As an example, given the success with LEDs, our system would lend itself to display technologies where it would obviate the need for row and column decoders. More powerfully, the ability to differentiate between receivers spaced so closely together has a direct impact on increasing the channel capacity of, for example, near field radio frequency identification (RFID) systems; in a very small space, multiple channels can be addressed independently. Finally, the techniques here can be applied to enhancing the resolution of RF imaging systems and image formation systems. Imaging is among the most compelling applications since the fundamental focusing is limited by the MM element size, not the wavelength of the RF energy as would traditionally be expected. In general, this work demonstrates a means to manipulate the electromagnetic energy in the near field, and so extends the possibilities of control of wave phenomena on a subwavlength scale.

[1]A. G. Cepni, "Experimental investigation of time-reversal techniques using electromagnetic waves," Ph.D. thesis (Carnegie Mellon University, 2005).
[2]G. Lerosey, J. de Rosny, A. Tourin, A. Derode, G. Montaldo, and M. Fink, Phys. Rev. Lett. **92**, 193904 (2004).
[3]B. E. Henty and D. D. Stancil, Phys. Rev. Lett. **93**, 243904 (2004).
[4]M. J. Chabalko, "Experimental investigation of time reversal with electromagnetic waves in the presence of random media," M.S. thesis (Carnegie Mellon University, 2008).
[5]Y. Jiang, J.-G. Zhu, D. D. Stancil, and M. J. Chabalko, in 2007 IEEE Antennas and Propagation Society International Symposium (2007).
[6]G. Lerosey, J. de Rosny, A. Tourin, and M. Fink, Science **315**, 1120 (2007).
[7]M. Fink, J. de Rosny, G. Lerosey, and A. Tourin, Compt. Rendus Phys. **10**, 447 (2009).
[8]F. Lemoult, G. Lerosey, J. de Rosny, and M. Fink, Phys. Rev. Lett. **104**, 203901 (2010).
[9]F. Lemoult, M. Fink, and G. Lerosey, Waves Random Complex Media **21**, 591 (2011).
[10]F. Lemoult, M. Fink, and G. Lerosey, Waves Random Complex Media **21**, 614 (2011).
[11]F. Lemoult, M. Fink, and G. Lerosey, Nat. Commun. **3**, 889 (2012).
[12]A. Ourir, G. Lerosey, F. Lemoult, M. Fink, and J. de Rosny, Appl. Phys. Lett. **101**, 111102 (2012).
[13]F. Lemoult, M. Fink, and G. Lerosey, Phys. Rev. Lett. **107**, 64301 (2011).
[14]M. J. Chabalko, W. C. Harris, D. D. Stancil, and D. S. Ricketts, in *2014 Asia-Pacific Microwave Conference* (2014), pp. 137–139.
[15]M. J. Chabalko and D. S. Ricketts, Appl. Phys. Lett. **106**, 62401 (2015).
[16]E. Shamonina and L. Solymar, J. Phys. Appl. Phys. **37**, 362 (2004).
[17]R. Syms, E. Shamonia, and L. Solymar, IEE Proc. Microwave Antennas Propag. **153**, 111 (2006).
[18]E. Bou-Balust, R. Sedwick, P. Fisher, and E. Alarcon, Wirel. Power Transfer **1**, 83–92 (2016).
[19]G. Lipworth, J. Ensworth, K. Seetharam, D. Huang, J. S. Lee, P. Schmalenberg, T. Nomura, M. S. Reynolds, D. R. Smith, and Y. Urzhumov, Sci. Rep. **4**, 3642 (2014).
[20]D. Huang, Y. Urzhumov, D. R. Smith, K. H. Teo, and J. Zhang, J. Appl. Phys. **111**, 64902 (2012).
[21]B. Wang, K. H. Teo, T. Nishino, W. Yerazunis, J. Barnwell, and J. Zhang, Appl. Phys. Lett. **98**, 254101 (2011).
[22]A. P. Sample, D. T. Meyer, and J. R. Smith, IEEE Trans. Ind. Electron. **58**, 544 (2011).
[23]T. C. Yang, IEEE J. Oceanic Eng. **28**, 229 (2003).